

# Gravitational-wave imaging of black hole horizons: Post-merger chirps from binary black holes

Juan Calderon Bustillo<sup>1,2,3</sup>, Chris Evans<sup>3</sup>, James A. Clark<sup>3</sup>, Grace Kim<sup>3</sup>, Pablo Laguna<sup>3</sup> and Deirdre Shoemaker<sup>3</sup>

<sup>1</sup>*Monash Centre for Astrophysics, School of Physics and Astronomy, Monash University, VIC 3800, Australia*

<sup>2</sup>*OzGrav: The ARC Centre of Excellence for Gravitational-Wave Discovery, Clayton, VIC 3800, Australia*

<sup>3</sup>*Center for Relativistic Astrophysics and School of Physics, Georgia Institute of Technology, Atlanta, GA 30332*

**The merger of a binary black hole gives birth to a highly distorted remnant black hole that relaxes to its final state by emitting gravitational waves. During this fraction of a second, space-time provides us with a unique opportunity to probe the most extreme regime of gravity by studying the behaviour highly dynamical black hole horizons. In this article, we show for the first time how a concrete geometrical feature of the evolving horizon imprints the gravitational-wave emission. We find that the line-of-sight passage of a “cusp”-like defect present on the remnant horizon of asymmetric binary black hole mergers correlates with post-merger “chirp” signatures in the observed gravitational-waves. While the Event Horizon Telescope has produced the most direct image of a mature, relatively sedate black hole, Advanced LIGO and Virgo may soon examine the horizon itself of dynamical newborn ones.**

A new field of astronomy has arisen after the detection of gravitational waves (GWs). To date, Advanced LIGO <sup>1</sup> and Virgo <sup>2</sup> have observed the waves emitted by the coalescence of ten binary black holes (BBHs) <sup>3,4</sup> and one binary neutron star <sup>5</sup>. GWs are allowing us to explore the nature of these exotic objects, their population <sup>6</sup> and their formation channels <sup>7,8</sup>. These observations are also confirming that Einstein’s theory of General Relativity (GR) <sup>9,10</sup> is likely the correct theory of gravity <sup>11–13</sup>. Despite this groundbreaking achievement, the properties of current BBH detections have prevented to observe in detail their merger and post-merger emission, when gravity is at its most violent and dynamic regime. As the GW detector network expands and improves its sensitivity, the GWs emitted during these fractions of a second will provide a unique chance to observe the dynamical properties of highly distorted BH horizons, understanding strong gravity phenomena like the gravitational recoil (or *kick*) <sup>14,15</sup>, and testing fundamental aspects of GR like the “no-hair” theorem <sup>10</sup>.

Any of the mentioned studies will rely on a deep understanding of how the properties of the source determine the morphology of the GWs. The coalescence of a non-precessing BBH produces relatively simple GWs (Fig.1, middle row, left panel). First, the frequency and amplitude of these signals grow monotonically as the two BHs orbit and approach each other <sup>16</sup>. Next, when the two objects are about to merge, their speeds become comparable to that of light, causing a fast rise of both the frequency and amplitude of the signal <sup>16,17</sup>. Finally, after a highly distorted black hole has formed, this settles to a Kerr black hole emitting exponentially decaying ringdown radiation <sup>18,19</sup>

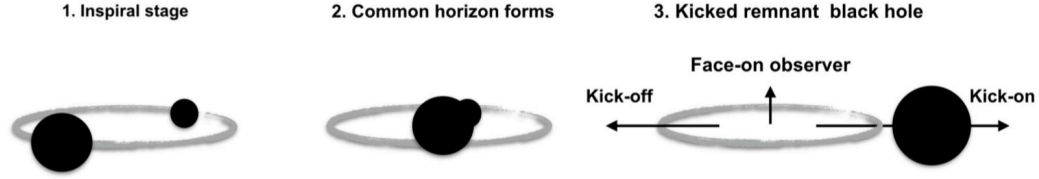
of constant frequency. The resulting signal morphology is known as *chirp* and is consistent with all BBH observations so far <sup>4</sup>. In contrast, in this article we show that this simple morphology is only true when the BBH components have comparable masses or it is viewed face-on so that the GW emission is vastly dominated by its so called quadrupole mode. This is the case for all current observations.

Unlike current BBH detections, asymmetric BBHs <sup>1</sup> show strong secondary GW emission modes. These are strongly triggered during the BBH merger and ringdown stages <sup>20</sup> and lead to a complex post-merger waveform morphology, not observed in current detections, that can be exploited to study the dynamic properties of the final black hole <sup>15</sup> (Fig. 1). Here we show the first example of such complex post-merger emission and how it reflects the dynamics of the evolving newborn BH. In particular, we show that multiple frequency peaks (or *chirps*) can be observed in the post-merger emission of unequal mass binaries when the observer is located near the orbital plane. Using state-of-the-art numerical-relativity simulations, we find that these chirps are produced as large curvature gradient regions, surrounding the “cusp” of the newborn BH horizon, cross the line of sight. In contrast, frequency minima happen as the wider “back” region of the horizon, where the curvature gradient is smaller, crosses the line-of-sight.

---

<sup>1</sup>In this article we restrict to non-spinning BBHs, so that we refer as asymmetric binaries to those formed by unequal mass BHs.

**A. Stages of a binary black hole coalescence:**



**B. Gravitational-wave signals. Top: Mass ratio  $q=3$ , varying observer location. Bottom: Varying  $q$ , fixed observer location.**

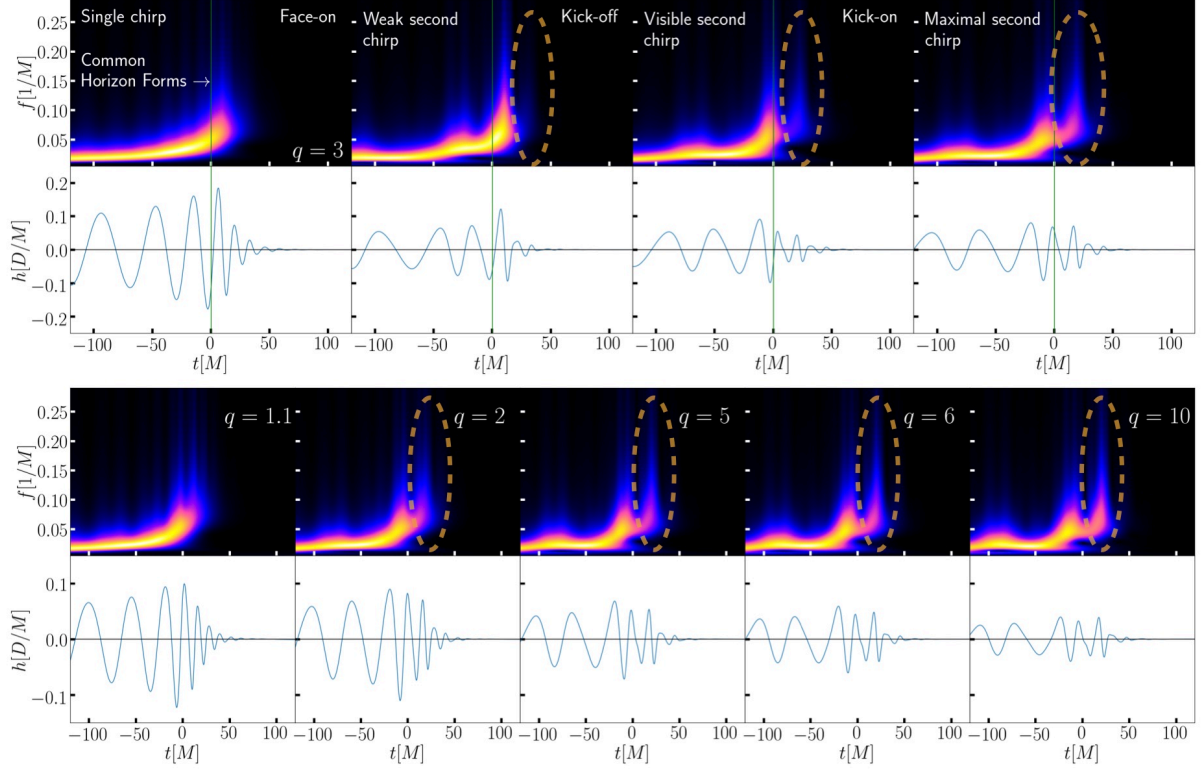


**Figure 1: Post-merger secondary chirps from edge-on binaries.** The top panels show the time series (white background) and time frequency maps (black background) of simulated gravitational-wave strain  $h(t)$  emitted by a  $q = 3$  non-spinning binary, as observed from different locations around the binary. The green vertical bar denotes the time at which the final common horizon is first found in the simulation. The top left panel shows the signal observed by a face-on observer, which shows a canonical *single chirp* structure. The next two panels show the signals emitted in

the direction in which the final remnant black hole is ejected, and the one opposite to it. In these, a faint *secondary chirp*, emitted after the common horizon is formed, is visible. The rightmost plot shows the signal observed  $55^\circ$  away from the kick direction, for which a clear *double chirp* is visible. The bottom panel shows the signals emitted in this same direction for the case of binaries of varying mass ratio. In all cases, a secondary post-merger chirp can be observed. This is more clear for increasing mass ratio  $q$ . All waveforms include the most dominant gravitational-wave modes  $(\ell, |m|) = \{(2, 1), (2, 2), (3, 2), (3, 3), (4, 3), (4, 4)\}$

## 1 Multiple post-merger chirps

The second row of Fig. 1 shows the strain (bottom) and time-frequency maps (top) of GW signals extracted from a numerical simulation of a non-spinning binary with mass ratio  $q = 3$ <sup>2</sup>. The first vertical blue line denotes the moment at which the final common apparent horizon is formed. In the leftmost plot, the source is observed face-on and the signal has a canonical single chirp structure. The next three plots show signals measured by observers placed at different positions within the orbital plane. After the common horizon has formed, some of the observers measure a clear drop of the frequency followed by a secondary post-merger chirp. Notably, different observers do not only see these post-merger chirps at different times but also measure different amplitude and frequency peaks. It is illustrative to compare the signals measured by the observer located on the direction to which the final black hole is kicked (kick-on) and on the opposite one (kick-off)<sup>14,15</sup>.

---

<sup>2</sup>All simulations used in this work have been produced with Gatech’s Maya code<sup>21</sup>. The Maya code uses the Einstein Toolkit<sup>22</sup> which is based on the CACTUS<sup>23</sup> infrastructure and CARPET<sup>24</sup> mesh refinement.

In the case we consider, the kick-off observer measures a first chirp that has large amplitude and frequency peaks, and later measures a much weaker second chirp, difficult to spot in the Figure. In contrast, the kick-on observer records a first chirp of smaller amplitude and frequency peaks than the kick-off one, but records a more clear secondary chirp. We find that the intensity of this secondary chirp is strongest for an observer located on the orbital plane,  $55^\circ$  away from the kick direction (rightmost panel). In fact, we find that this *double chirp* structure is most prominent for this kind of observer for a wide range of BBHs of varying mass ratio, as shown in the bottom row of Fig. 1.

The complex GW strain emitted in a direction  $(\iota, \varphi)$  on the sky of a binary black hole merger can be written as a superposition of different GW modes  $h_{\ell,m}(\iota, \varphi; t)$  as  $h(t) = h_+(t) - ih_\times(t) = \sum_{\ell,m} Y_{\ell,m}^{-2}(\iota, \varphi) h_{\ell,m}(t)$ . Here,  $h_+$  and  $h_\times$  denote the two GW polarizations, the  $Y_{\ell,m}$ 's are spin-2 weighted spherical harmonics and  $(\iota, \varphi)$  are the polar and azimuthal angles of a spherical coordinate system centred on the binary. The direction  $\iota = 0$  (face-on) denotes the direction of the orbital angular momentum, with the orbital plane of the binary located at  $\iota = \pi/2$  (edge-on). During the inspiral stage, the frequency  $f_{\ell,m}$  of each mode goes as  $f_{\ell,m} \sim m f_{orb}$ , with  $f_{orb}$  denoting the orbital frequency of the binary. After the merger, each mode settles to a constant ringdown frequency  $f_{\ell,m}^R$ . For face-on binaries, the quadrupolar  $(\ell, m) = (2, \pm 2)$  modes vastly dominates during all the stages of the binary. As consequence, the frequency of the resulting GW is, to a good approximation twice the orbital one and the observed signal shows a canonical single chirp morphology. Higher GW modes are triggered during the merger and ringdown stages and are visible near the

orbital plane of the binary (i.e., for nearly edge-on sources). The complicated interactions of these modes lead to the rich and complicated waveform morphologies showed in Fig.1 and in particular to the secondary post-merger chirps. Hence, in analytical terms, the post-merger chirps can be explained as just the result of these complicated interactions. However, such an evident feature suggests the existence of a clear post-merger phenomena that explains its origin. In other words, we ought to spot a concrete feature of the evolving source that triggers the secondary chirps. As we will show, this feature is the existence of a cusp in the apparent horizon of the remnant black hole that repeatedly points to each of the observers as it fades away, resembling a sort of fading gravitational-wave lighthouse.

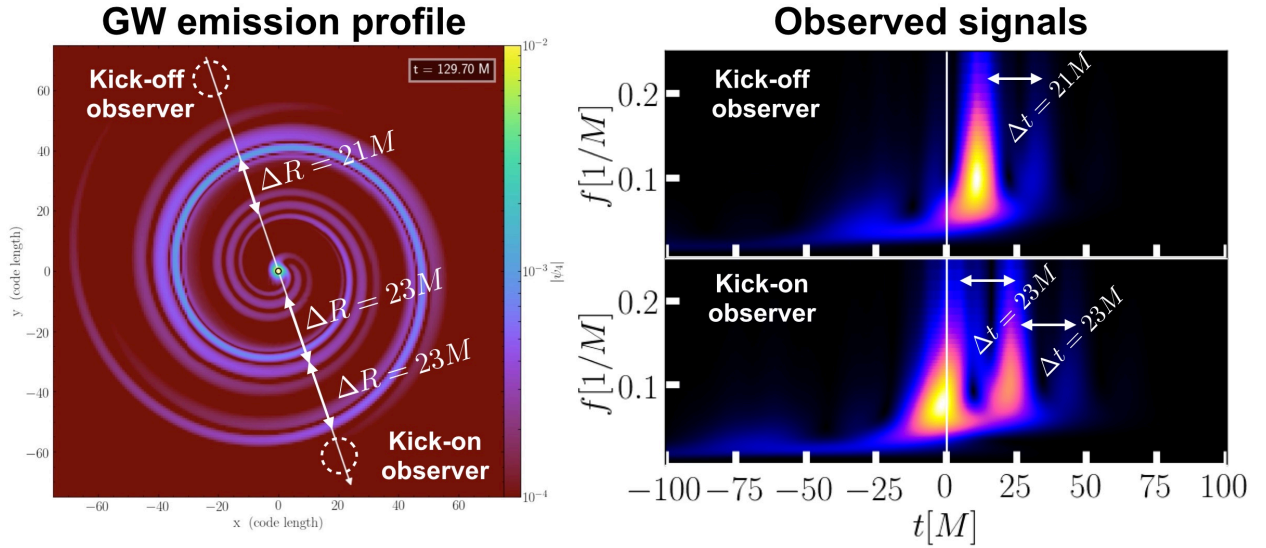


Figure 2: **Post merger emission observed far from the source.** The left panel shows the absolute value of  $\psi_4$  on the orbital plane of non-spinning  $q = 3$  binaries. Two strong tight wave-fronts separated by approximately  $\sim 20M$  travel toward the observer located on the bottom of the panel, in the kick-on direction. This observer measures two strong chirps separated by a time difference

consistent with the spatial separation of the traveling fronts. This is shown in the bottom right panel for the case of the kick-on observer, who measures a clear *double chirp* and a much weaker third chirp, whose time of arrival is again consistent with the spatial separation of the traveling wavefronts. In contrast, the second front traveling toward the kick-off observers is much weaker than in the kick-on case, leading to a weak second chirp.

## 2 Physical origin of the post-merger chirps: far from the source

The left panel of Fig.2 shows the post-merger gravitational-wave emission on the orbital plane of the  $q = 3$  non-spinning binary from Fig.1, after the waves have traveled far from the source. We represent this by the Newmann-Penrose scalar  $\psi_4$ <sup>25</sup>, related to the GW strain  $h$  by  $\psi_4(t) = \frac{d^2 h(t)}{dt^2}$ . The emission pattern it is clearly asymmetric, so that different observers record very different GW signals as we showcase this in the right panels for the case of the kick-on and kick-off observers. Each of these receives several GW wave-fronts spatially separated by approximately  $\Delta R \sim \mathcal{O}(20M)$ , consistent with the time difference  $\Delta t$  between the frequency peaks (or chirps) they record<sup>3</sup>. The intensity of these fronts is clearly different the two observers. While the kick-on observer receives up to two wave-trains of similar intensity, the second train reaching the kick-on observer has a much lower intensity as a result of the progressive decaying GW emission of the source. Due to this, the kick-on observer measures two chirps of similar intensity plus a weak third one while the second chirp is barely visible for the kick-off observer.

---

<sup>3</sup>Note that in geometric units, the speed of light, and hence that of GWs, is  $c = 1$



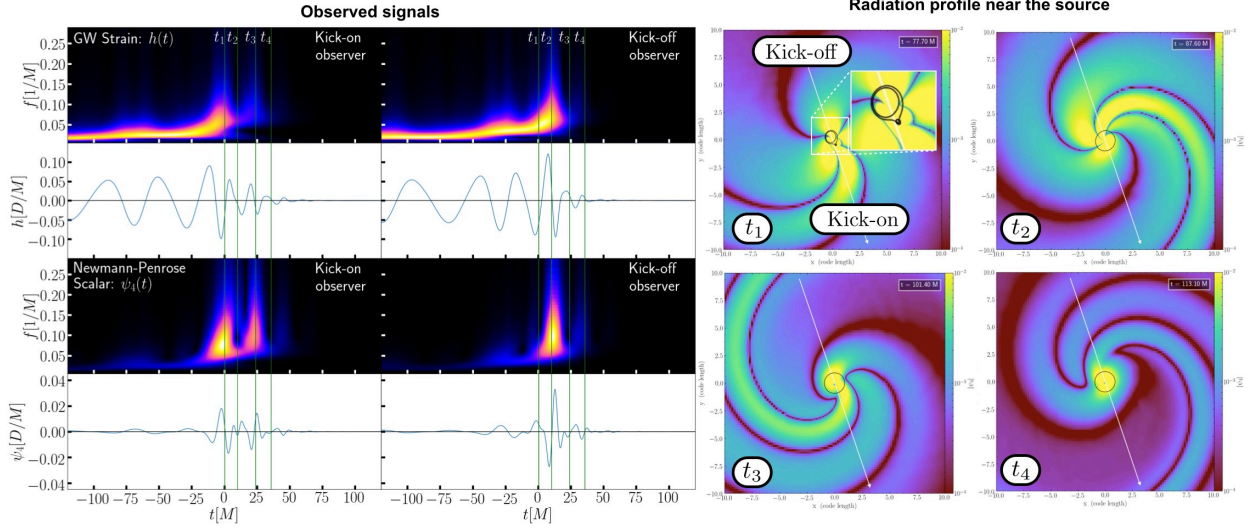


**Figure 3: Relation between frequency and near horizon emission via retarded times.** The two top (bottom) rows of the left figure show the time-domain gravitational-wave strain ( $\psi_4$ ) and time-frequency maps recorded by two observers located on the orbital plane of a non-spinning  $q = 3$  binary black hole. The left cases correspond to an observer located in the direction of the final kick while right ones correspond to an observer located  $180^\circ$  away. The vertical lines denote four selected times  $t_{i,GW}$  at which the recorded signal shows a frequency peak for one observer and a minima for the other. The right panels show the  $\psi_4$  profile around the final BH at four selected times  $t_{i,Frame} = t_{i,GW} + 77M$ . In these, the central beam (wider back) of the  $\psi_4$  trident structure points to the observer measuring the frequency peak (minima) at  $t_{i,GW}$ . The two frames are precisely related by  $t_{GW} = t_{Frame} + 77M$ .

### 3 Physical origin of the post-merger chirps: near the black hole horizon

Next, we study the radiation profile near the source to find a link between it and the measured GWs. To this, we zoom in our simulation to resolve  $\psi_4$  close to the final apparent horizon. The left panels of Fig.3 shows the GW strain (top) and  $\psi_4$  (bottom) time series and time-frequency maps measured by the kick-on and kick-off observers. The four green vertical lines denote four selected times  $t_{i,GW}$ , at which the two selected observers measure either a chirp or a frequency minima. The right panels show the near horizon  $\psi_4$  profile at times  $t_{i,Frame} = t_{i,GW} + 77M$ , where  $77M$  is the time delay relating both frames of reference.<sup>4</sup> In all of these, the common apparent horizon, highlighted in panel  $t_1$ , has already formed and has initially a very asymmetric *chestnut* shape: while a sharp, highly curved *cusp* forms in one region, the opposite side of the horizon shows a lower curvature. Accordingly,  $\psi_4$  shows a very clear pattern; a *trident* composed by three radiation beams of high intensity forms in the region surrounding the cusp, while a wider and weaker beam forms on the opposite side.<sup>5</sup> Panels  $t_2$  to  $t_4$  show how this structure rotates as the highly distorted final horizon relaxes to a Kerr black hole. As this happens, the  $\psi_4$  trident structure faces all the different observers, leading to the triple wavefronts in Fig. 2 that lead to the chirps measured far from the source. In this process, the components of the  $\psi_4$  structure vary both their separation and intensity, leading to varying frequency and amplitude peaks of the chirps measured by different observers. The intensity of the central lock of the trident raises for some time

---

<sup>4</sup>This delay is not arbitrary: we obtain it by finding the time at which the anti-kick phenomenon<sup>26</sup> is measured in each of the frames.

<sup>5</sup>We note that this structure does not form abruptly in the moment at which the common horizon appears. Instead, it forms progressively as the two black holes approach each other.

after the merger and is maximal approximately when it faces the kick-off direction. After this, the whole structure starts to fade away as the final black hole progressively settles to a Kerr one. In doing so, the fading trident structure still faces again several observers with enough intensity that the corresponding radiation can be measured in the far zone. This leads to the second wave-train described in Fig.2 and the observation of a second chirp.

#### 4 The origin of the $\psi_4$ structure: linking chirps to the geometry of the final horizon

In the first frame shown in Fig. 3, it seems evident that the  $\psi_4$ -trident structure is located on the region of the horizon surrounding its cusp, suggesting that it is this feature what leads to the chirps. However, it is impossible to verify this throughout its whole evolution by simple visual inspection. In this section we confirm this hypothesis by finding that the intensity of the radiation measured on the black hole horizon is related to the *gradient of its curvature*, which precisely shows three maxima around the location of the cusp.

Our point of departure are existing results coming from the modelling of head-on black hole collisions <sup>26</sup>. According to these, large curvature regions of the final black hole horizon have a larger linear momentum flux than those of low curvature (measured as the *Gaussian curvature*  $K$  of the horizon, intrinsic to the surface <sup>26</sup>). Although a large momentum flux does not necessarily correspond to a large  $|\psi_4|$ , we started by comparing these two quantities on the final horizon. While we find with that  $K$  does always peak roughly at the location of the maximum of  $\psi_4$ , it fails to reproduce the multiple local maxima and minima of  $|\psi_4|$ . Next, we adopt a different approach

by comparing  $\psi_4$  to the derivative of the *Mean curvature*  $H$  along the horizon. Two reasons motivate this choice. First, unlike  $K$ ,  $H$  depends on the way that the event horizon is embedded in its ambient space-time, and it seems natural that the GW emission will depend on the final BH environment. Second, the final horizon evolves to its final state by eliminating not its horizon curvature but defects on it; a naive way to describe these defects is that of gradients of its curvature with respect to its arc-length  $dH/ds$ . Consequently, Fig.4 shows the value  $|\psi_4|$  and  $|dH/ds|$  on the intersection of the final horizon with the orbital plane of the binary  $4.70M$  after the common horizon forms. The colour panel shows the corresponding simulation frame, with the colour code denoting the intensity of  $|\psi_4|$ . Note that  $dH/ds$  does not only peak at  $\varphi = \pi/8$ , where the central beam of the trident is located, but also shows local maxima and minima at locations matching those of  $\psi_4$ . In particular, it is clear that the three close maxima producing the trident structure leading to the chirps coincide with three local peaks of  $dH/ds$ . While this relation does not hold perfectly during the whole evolution of the final black hole, the peak of  $dH/ds$  always captures that of  $\psi_4$ . This allows us to establish a correlation between the location of the trident structure on the horizon with that of the region of the horizon with the highest curvature gradient, which we refer to as *cusp*.

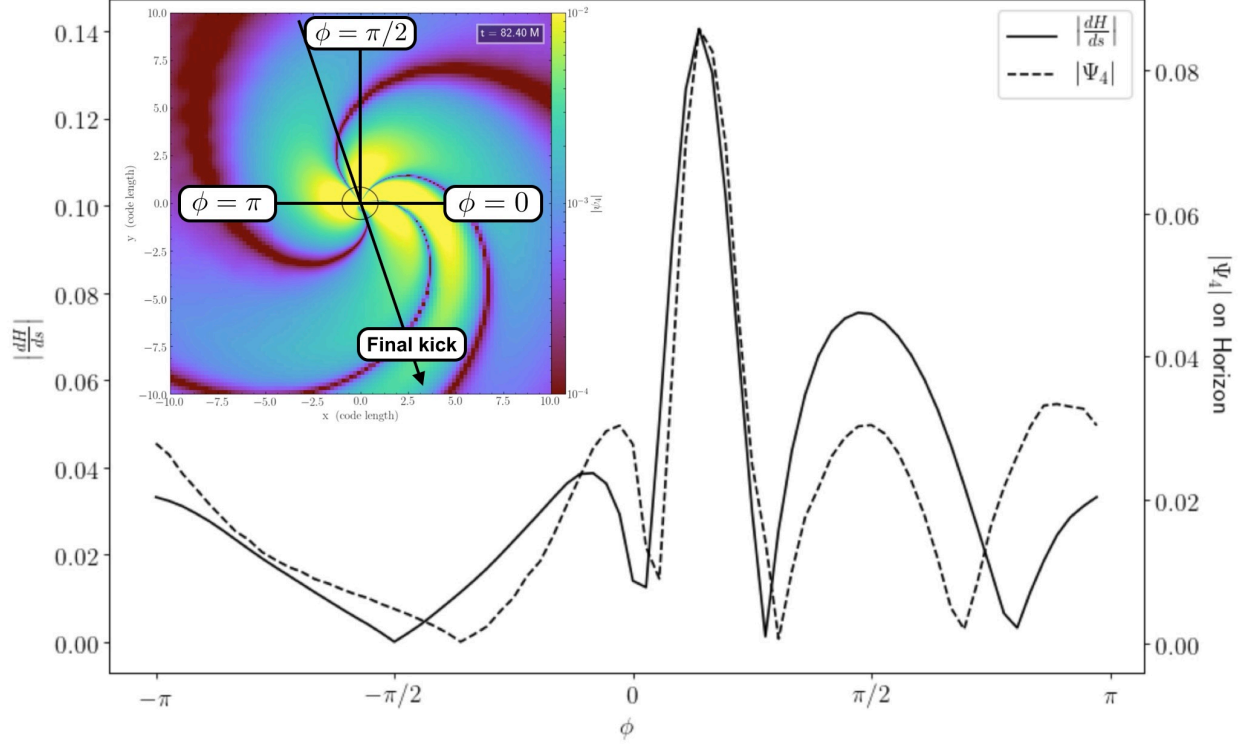


Figure 4: **Relation between the curvature of the final event horizon and the intensity of the gravitational wave emission.** Absolute value of  $\psi_4$  (dashed) and gradient of the mean curvature  $H$  (solid) measured on the intersection final horizon with the orbital plane. The data is read  $4.70M$  after the common horizon is formed. The top left panel shows the corresponding frame of our numerical simulation. The minima and maxima of both quantities coincide to good accuracy. Moreover, the peak of of the gradient of  $H$  matches that of  $\psi_4$ . While this relation is not perfect, we observe a tight correlation between the two quantities.

Our results show that the observation of post-merger chirps is reflects the passage through the line-of-sight of the cusp of the final horizon formed after the collision of an unequal mass binary. In the past, it has been shown that there exists a correlation between the behaviour of the horizon and the

waveform observed far away from the black hole <sup>27</sup>. However, while this connection has always been established in terms of non directly measurable quantities like GW flux and multipoles <sup>26,28–30</sup>, our finding constitutes the first link between a concrete, observable feature of a gravitational wave signal and a concrete geometric feature of the horizon of the final black hole horizon.

## 5 Observability of post merger chirps

In this section we estimate the distance at which a secondary post-merger chirp can be observed for several kinds of binaries. To this, we require that the second chirp alone produces a signal-to-noise ratio (SNR) of at least  $\rho = 5$ , which would represent a  $5\sigma$  deviation from Gaussian noise <sup>31</sup>. Fig. 5 shows the distance at which the second chirp of an optimally oriented binary (with the observer sitting on its orbital plane and  $55^\circ$  away from the kick direction) can produce an SNR of 5. We show this for the case of four families of binaries with different mass ratios and varying total mass. We consider a single Advanced LIGO detector working at both the achieved sensitivity during its second observing run <sup>32</sup> (solid) and at its design sensitivity (dashed) <sup>33</sup>. We find that very nearby sources, closer than  $d_H = 400 Mpc$ , would be needed to clearly resolve the second post-merger chirp during the second Advanced LIGO run. However, this may be observable up to distances of  $d_H = 3 Gpc$  once Advanced LIGO reaches its design sensitivity for the case of edge-on intermediate mass black hole binaries of  $150 M_\odot$  with a mass ratio  $q \geq 2$ . We note that no such a source has been yet observed <sup>4,34</sup> and that such detection represents a great challenge for gravitational-wave searches <sup>35–40</sup>. However, the dramatic increase in sensitivity in the low frequency band that Advanced LIGO will undergo once it reaches its design sensitivity <sup>33</sup> and the

development of dedicated searches for these sources<sup>41</sup> might enable the first observation of double chirps in the near future.

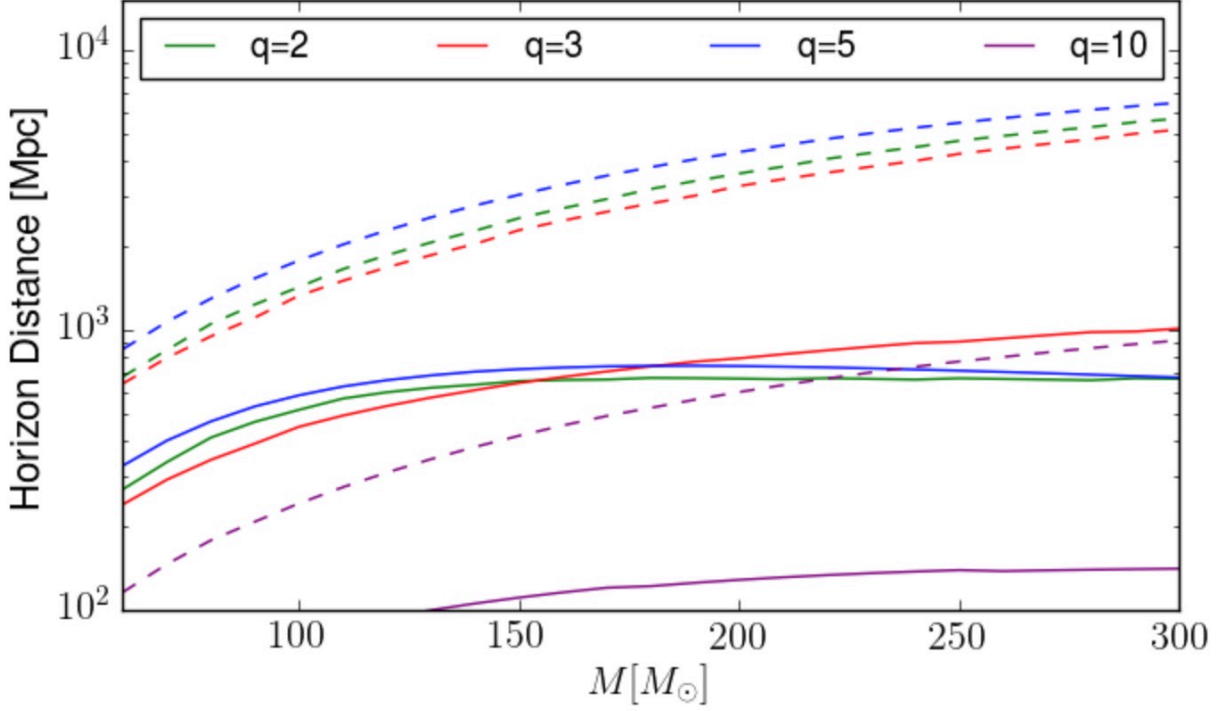


Figure 5: **Observability of post-merger black hole chirps.** The right plot shows the distance at which the secondary chirps from the remnant of a several non-spinning binary can produce a signal-to-noise ratio of 5, as a function of the total mass of the binary. Our results consider a single Advanced LIGO detector working at its early sensitivity (solid) and design sensitivity (dashed). We consider only the case in which the secondary chirp is most intense, namely  $(\iota, \varphi) = (\pi/2, 11\pi/36)$  and choose optimal sky-location. We consider a low frequency cutoff of  $f_0 = 10\text{Hz}$ . At design sensitivity, Advanced LIGO can see the secondary chirp of a  $q \leq 5$  binary at a distance of  $\sim 0.8\text{Gpc}$  if the mass of the total binary is  $M \sim 60M_\odot$ .

## 6 Conclusions

To date, Advanced LIGO and Virgo have observed the gravitational waves emitted by the coalescence of ten binary black holes, enabling the first studies of gravity in its strongest field regime. Understanding how the evolving geometry of the remnant black hole imprints the observed gravitational-wave emission will be key to understand gravity in its most extreme form. While past work has suggested that these imprints might exist<sup>26,28–30</sup>, in this article we have identified for the first time one of them: the presence of multiple post-merger frequency peaks in the observed post-merger signal, which we refer to as *post-merger chirps*. These chirps can be observed near the orbital plane of asymmetric binaries in directions close to the traveling direction of the final black hole, also known as *kick direction*. We have found that these chirps have their origin in the passage by the line of sight of the fading cusp formed on the remnant black hole of asymmetric black hole mergers, posing the first direct link between a concrete geometrical feature of the horizon of a black hole and a concrete feature in the observed gravitational waves.

The recent observation by the Event Horizon Telescope of the shadow of the super-massive black hole M87 has provided the most direct image of a black hole thus far, opening the gate directly observe long-existing and weakly perturbed black holes<sup>42,43</sup>. Our findings indicate that gravitational-waves will allow us to dig even deeper and resolve the evolving structure of the horizon itself of newborn and fully dynamical ones.



## Acknowledgements

We thank Paul Lasky and Valentin Christiaens for comments on the manuscript. The authors gratefully acknowledge support from the NSF grants 1505824, 1505524, 1550461, XSEDE TG-PHY120016. JCB also acknowledges support from Australian Research Council Discovery Project DP180103155. This research was also supported in part through research cyberinfrastructure resources and services provided by the Partnership for an Advanced Computing Environment (PACE) at the Georgia Institute of Technology<sup>44</sup>. The results in Section 5 made use of the Python Numerical Relativity Injection infrastructure described in<sup>45</sup>. This manuscript has LIGO DCC number P1900139.

## References

1. Aasi, J. *et al.* Advanced LIGO. *Class. Quant. Grav.* **32**, 074001 (2015). 1411.4547.
2. Acernese, F. *et al.* Advanced Virgo: a second-generation interferometric gravitational wave detector. *Class. Quant. Grav.* **32**, 024001 (2015). 1408.3978.
3. Abbott, B. P. *et al.* Observation of Gravitational Waves from a Binary Black Hole Merger. *Phys. Rev. Lett.* **116**, 061102 (2016). 1602.03837.
4. Abbott, B. P. *et al.* GWTC-1: A Gravitational-Wave Transient Catalog of Compact Binary Mergers Observed by LIGO and Virgo during the First and Second Observing Runs (2018). 1811.12907.

5. Abbott, B. P. *et al.* GW170817: Observation of Gravitational Waves from a Binary Neutron Star Inspiral. *Phys. Rev. Lett.* **119**, 161101 (2017). 1710.05832.
6. Abbott, B. P. *et al.* Binary Black Hole Population Properties Inferred from the First and Second Observing Runs of Advanced LIGO and Advanced Virgo (2018). 1811.12940.
7. Abbott, B. P. *et al.* Astrophysical Implications of the Binary Black-Hole Merger GW150914. *Astrophys. J.* **818**, L22 (2016). 1602.03846.
8. Stevenson, S. *et al.* Formation of the first three gravitational-wave observations through isolated binary evolution (2017). [Nature Commun.8,14906(2017)], 1704.01352.
9. Einstein, A. The Foundation of the General Theory of Relativity. *Annalen Phys.* **49**, 769–822 (1916). [Annalen Phys.14,517(2005)].
10. Misner, C. W., Thorne, K. & Wheeler, J. Gravitation (1974).
11. Abbott, B. P. *et al.* Tests of General Relativity with the Binary Black Hole Signals from the LIGO-Virgo Catalog GWTC-1 (2019). 1903.04467.
12. Abbott, B. P. *et al.* Tests of general relativity with GW150914. *Phys. Rev. Lett.* **116**, 221101 (2016). 1602.03841.
13. Abbott, B. P. *et al.* Binary black hole mergers in the first advanced ligo observing run. *Phys. Rev. X* **6**, 041015 (2016). URL <https://link.aps.org/doi/10.1103/PhysRevX.6.041015>.

14. Gonzalez, J. A., Sperhake, U., Bruegmann, B., Hannam, M. & Husa, S. Total recoil: The Maximum kick from nonspinning black-hole binary inspiral. *Phys. Rev. Lett.* **98**, 091101 (2007). [gr-qc/0610154](#).
15. Calderón Bustillo, J., Clark, J. A., Laguna, P. & Shoemaker, D. Tracking black hole kicks from gravitational wave observations. *Phys. Rev. Lett.* **121**, 191102 (2018). [1806.11160](#).
16. Husa, S. Michele Maggiore: Gravitational waves. Volume 1: Theory and experiments. *Gen. Rel. Grav.* **41**, 1667–1669 (2009).
17. Pretorius, F. Evolution of binary black hole spacetimes. *Phys. Rev. Lett.* **95**, 121101 (2005). [gr-qc/0507014](#).
18. Berti, E., Cardoso, V. & Starinets, A. O. Quasinormal modes of black holes and black branes. *Class. Quant. Grav.* **26**, 163001 (2009). [0905.2975](#).
19. Owen, R. The Final Remnant of Binary Black Hole Mergers: Multipolar Analysis. *Phys. Rev.* **D80**, 084012 (2009). [0907.0280](#).
20. Berti, E. *et al.* Inspiral, merger and ringdown of unequal mass black hole binaries: A Multipolar analysis. *Phys. Rev. D* **76**, 064034 (2007). [gr-qc/0703053](#).
21. Haas, R., Shcherbakov, R. V., Bode, T. & Laguna, P. Tidal Disruptions of White Dwarfs from Ultra-Close Encounters with Intermediate Mass Spinning Black Holes. *Astrophys. J.* **749**, 117 (2012). [1201.4389](#).
22. Einstein toolkit: <http://www.einsteintoolkit.org>.

23. Cactus: <http://www.cactuscode.org>.
24. Schnetter, E., Hawley, S. H. & Hawke, I. Evolutions in 3-D numerical relativity using fixed mesh refinement. *Class. Quant. Grav.* **21**, 1465–1488 (2004). [gr-qc/0310042](#).
25. Newman, E. & Penrose, R. An Approach to gravitational radiation by a method of spin coefficients. *J. Math. Phys.* **3**, 566–578 (1962).
26. Rezzolla, L., Macedo, R. P. & Jaramillo, J. L. Understanding the 'anti-kick' in the merger of binary black holes. *Phys. Rev. Lett.* **104**, 221101 (2010). [1003.0873](#).
27. Gupta, A., Krishnan, B., Nielsen, A. & Schnetter, E. Dynamics of marginally trapped surfaces in a binary black hole merger: Growth and approach to equilibrium. *Phys. Rev.* **D97**, 084028 (2018). [1801.07048](#).
28. Jaramillo, J. L., Macedo, R. P., Moesta, P. & Rezzolla, L. Black-hole horizons as probes of black-hole dynamics II: geometrical insights. *Phys. Rev.* **D85**, 084031 (2012). [1108.0061](#).
29. Jaramillo, J. L., Panosso Macedo, R., Moesta, P. & Rezzolla, L. Black-hole horizons as probes of black-hole dynamics I: post-merger recoil in head-on collisions. *Phys. Rev.* **D85**, 084030 (2012). [1108.0060](#).
30. Jaramillo, J. L., Macedo, R. P., Moesta, P. & Rezzolla, L. Towards a cross-correlation approach to strong-field dynamics in Black Hole spacetimes. *AIP Conf. Proc.* **1458**, 158–173 (2012). [1205.3902](#).

31. Wainstein, L. & Zubakov, V. Extraction of signals from noise. *Prentice-Hall, Englewood Cliffs* (1962).
32. Abbott, B. P. *et al.* Prospects for Observing and Localizing Gravitational-Wave Transients with Advanced LIGO, Advanced Virgo and KAGRA. *Living Rev. Rel.* **19**, 1 (2013). 1304.0670.
33. Shoemaker, D. *et al.* Advanced ligo anticipated sensitivity curves. *LIGO-T0900288*, <https://dcc.ligo.org/cgi-bin/DocDB/ShowDocument?docid=2974> (2010).
34. Abbott, B. P. *et al.* Search for intermediate mass black hole binaries in the first observing run of Advanced LIGO. *Phys. Rev.* **D96**, 022001 (2017). 1704.04628.
35. Capano, C., Pan, Y. & Buonanno, A. Impact of Higher Harmonics in Searching for Gravitational Waves from Non-Spinning Binary Black Holes. *Phys.Rev.* **D89**, 102003 (2014). 1311.1286.
36. Dal Canton, T., Bhagwat, S., Dhurandhar, S. & Lundgren, A. Effect of sine-Gaussian glitches on searches for binary coalescence. *Class.Quant.Grav.* **31**, 015016 (2014). 1304.0008.
37. Calderón Bustillo, J., Laguna, P. & Shoemaker, D. Detectability of gravitational waves from binary black holes: Impact of precession and higher modes. *Phys. Rev.* **D95**, 104038 (2017). 1612.02340.
38. Calderón Bustillo, J., Husa, S., Sintes, A. M. & Pürrer, M. Impact of gravitational radiation higher order modes on single aligned-spin gravitational wave searches for binary black holes. *Phys. Rev.* **D93**, 084019 (2016). 1511.02060.

39. Varma, V. & Ajith, P. Effects of nonquadrupole modes in the detection and parameter estimation of black hole binaries with nonprecessing spins. *Phys. Rev.* **D96**, 124024 (2017). 1612.05608.
40. Calderón Bustillo, J., Salemi, F., Dal Canton, T. & Jani, K. P. Sensitivity of gravitational wave searches to the full signal of intermediate-mass black hole binaries during the first observing run of Advanced LIGO. *Phys. Rev.* **D97**, 024016 (2018). 1711.02009.
41. Harry, I., Calderón Bustillo, J. & Nitz, A. Searching for the full symphony of black hole binary mergers. *Phys. Rev.* **D97**, 023004 (2018). 1709.09181.
42. Akiyama, K. *et al.* First M87 Event Horizon Telescope Results. I. The Shadow of the Supermassive Black Hole. *Astrophys. J.* **875**, L1 (2019).
43. Akiyama, K. *et al.* First M87 Event Horizon Telescope Results. VI. The Shadow and Mass of the Central Black Hole. *Astrophys. J.* **875**, L6 (2019).
44. PACE. "Partnership for an Advanced Computing Environment (PACE)". <http://www.pace.gatech.edu> (2017).
45. Schmidt, P., Harry, I. W. & Pfeiffer, H. P. Numerical Relativity Injection Infrastructure (2017). 1703.01076.